Journal of the European Ceramic Society **13** (1994) 355–363

High Temperature Compressive Tests of Aluminium Nitride: Mechanical Properties and Microstructure

I. Masson,[a,b] J. P. Feiereisen,[a] J. P. Michel,[a] A. George,[a] A. Mocellin[b]

[a] Laboratoire de Métallurgie Physique-Science des Matériaux, URA 155, [b] Laboratoire de Science et Génie des Matériaux Métalliques, URA 159, Ecole des Mines, Parc de Saurupt, 54042 Nancy Cedex, France.

&

P. Blumenfeld

Département RCI IRSID, B.P. 320, 57210 Maizieres-les-Metz, France

(Received 8 June 1993; revised version received 15 October 1993; accepted 10 November 1993)

Abstract

Sintered and hot-pressed AlN was tested in compression at high temperature (1500–1650°C) either in creep or constant strain rate experiments. The mechanical behaviour can be described with low stress exponents ($1 < n < 2$) and large apparent activation energies ($\gtrsim 600$ kJ/mol). Microstructural observations point to predominant intergranular deformation mechanisms, cavitation being especially important. Increased dislocation activity was seen in the grains when strain increased. Dislocations have basal Burgers vectors but glide in prismatic planes as well. Easy cross-slip is consistent with the observation of non-dissociated dislocations. At large stresses, screw dislocations are dominant.

Gesintertes und heißgepreßtes AlN wurde bei hohen Temperaturen (1500–1650°C) unter Anlegung einer Kompressionsspannung in Kriechexperimenten oder bei konstanten Dehnungsraten untersucht. Das mechanische Verhalten läßt sich durch einen kleinen Spannungsexponenten ($1 < n < 2$) und große scheinbare Aktivierungsenergien ($\gtrsim 600$ kJ/mol) beschreiben. Gefügeuntersuchungen deuten auf einen überwiegend intergranularen Verformungsmechanismus hin, mit besonderer Bedeutung der Hohlraumbildung. Bei Erhöhung der Dehnung konnte eine erhöhte Versetzungsaktivität in den Körnern beobachtet werden. Der Burgers-Vektor der Versetzungen liegt in der Basalebene, aber Gleitung in den Prismenebenen ist ebenso möglich. Die einfache Quergleitung idt in Übereinstimmung mit dem beobachteten Nichtdissoziieren der Versetzungen. Bei hohen Spannungen überwiegen Schraubenversetzungen.

Des expériences de compression à haute température (1500–1650°C) de deux qualités d'AlN, fritté et pressé à chaud, ont été réalisées par fluage et à vitesse de déformation constante. Le comportement mécanique de ce matériau peut être décrit par de faibles exposants de contrainte ($1 < n < 2$) et de fortes énergies d'activation ($\gtrsim 600$ kJ/mol). Les observations des microstructures montrent que les mécanismes de déformation intergranulaires, en particulier la cavitation, sont prédominants. Dans les grains, l'activité des dislocations croît avec la déformation. Les dislocations ont un vecteur de Burgers basal mais glissent également dans les plans prismatiques. Un glissement dévié facile est en accord avec l'observation de dislocations non dissociées. Pour les fortes contraintes, les dislocations vis sont majoritaires.

1 Introduction

Aluminium nitride is an iono-covalent material which crystallizes in the wurzite (2H) structure. High melting point (2400°C), excellent thermal conductivity and good resistance to molten metals together with oxidation resistance at high temperatures, make AlN an attractive material for use as special refractories in future equipment for metal processing. For such applications it is also necessary that sufficient mechanical property levels be achieved, in particular at high temperature.

AlN polycrystals were studied at ambient temperature under uniaxial compression under a confining pressure up to 1·25 GPa and at strain rates between 3 and 7×10^{-5} s^{-1} by Heard & Cline.[1] Stress–strain

Journal of the European Ceramic Society 0955-2219/94/$7.00

curves showed a brittle–ductile transition at 0·55 GPa and the ultimate strength increased from 3·26 GPa to 4·7 GPa under 0·1 GPa to 0·8 GPa confining pressures respectively. After testing, TEM observations revealed a high density of dislocations parallel to the traces of all three *a*-axes.

Audurier *et al.*[2,3] have also deformed AlN specimens containing 1 to 20 wt% Y_2O_3 at constant strain rate of $2 \times 10^{-5}\,s^{-1}$ under confining pressures 0·7 to 1 GPa between room temperature and 800°C. The purpose of their work was to study dislocation substructures by TEM in samples deformed 1 to 2%. They concluded that basal and prismatic planes are easy glide planes. Dislocations had a Burgers vector 1/3 $\langle 11\bar{2}0 \rangle$ type and dominant screw orientation in the temperature range investigated. Boch *et al.*[4] carried out creep tests in three-point bending up to 1300°C under a stress of 190 MPa on hot-pressed AlN densified without additives. It has been found that at 1000°C for up to 100 h, the dense material exhibits only primary and steady-state creep behavior. The strain rate was found to be roughly proportional to the square of the applied stress. This result was considered evidence that no liquid second phase influences the grain boundary sliding.

Creep experiments in four-point bending were also performed on hot-pressed aluminium nitride samples of grain sizes between 1·8 and 19 μm by Jou & Virkar.[5] The outer fibre stress was varied between 20 and 140 MPa and the temperature between 1377 and 1667°C. The stress exponent, n, varied from 1·27 to 1·43, and the mechanism of creep was suggested to be diffusional. The grain size exponent, p, was found to be approximately between 2·2 and 2·4. Furthermore, the activation energy ranged between 529 and 625 kJ/mol. TEM observations did not show a noticeable change in the dislocation density but cavitation was observed in the deformed samples.

It therefore appears from this brief review of the literature that creep and deformation behaviour of AlN ceramics remain poorly documented and insufficiently understood. Therefore it is the purpose of this paper to report on some experiments and briefly discuss their significance in the light of the structural changes observed to take place in the samples.

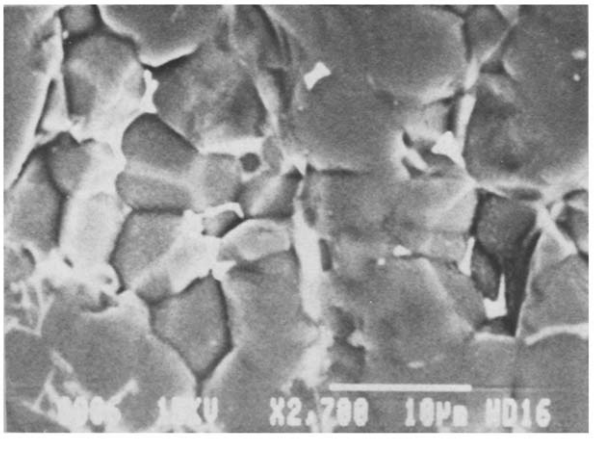

Fig. 1. As-received SAlN. SEM micrograph (back-scattered electrons). The second phase appears with bright contrast at some grain boundaries and triple points.

In this context, two types of tests have been carried out on sintered and hot-pressed aluminum nitrides (respectively SAlN and HPAlN):

—creep in compression,
—compression at low constant strain rate (called thereafter CSR),

at temperatures from 1500 to 1650°C in argon and helium gases.

2 Experimental Procedure and Materials

Commercial disks of SAlN and HPAlN 130 and 200 mm diameter respectively were obtained from ESK (ElectroSchmelzwerk Kempten GmbH, Germany). These materials have been prepared with a sintering additive forming a second phase under sintering conditions.

A chemical analysis using an inductively coupled plasma showed the presence of about 2 wt% of lanthanum in SAlN and HPAlN which corresponds to a volume fraction of nearly 5% as the oxide. The main phase detected by X-ray diffraction (XRD) ($CoK_{\alpha 1}$ radiation) and EDX was lanthanum aluminate ($La_2O_3.11\ Al_2O_3$). Scanning electron microscopy (SEM) examination (Fig. 1) reveals the second-phase distribution and allows for grain size measurements by the linear intercept method. This method applied to a population of 200 grains leads to the following average grain diameters, $d = 6{\cdot}9 \pm 2{\cdot}4\,\mu m$ for SAlN and $4{\cdot}1 \pm 1{\cdot}8\,\mu m$ for HPAlN respectively.

For TEM observations, thin foils were made by mechanical polishing and dimple grinding followed by ion thinning to perforation, and were examined in a JEOL 200 CX electron microscope operating at 200 kV and in a Philips CM12 electron microscope operating at 120 kV for EDS analysis. For both materials, second phases were observed as dark particles at triple points and grain boundaries. Few individual dislocations were found in the grains (Fig. 2). The three possible Burgers vectors 1/3 $\langle 11\bar{2}0 \rangle$ in the basal plane were observed; no dissociation into partials was detected by the weak-beam technique. Sometimes perfect dislocations were found to be arranged in subgrain boundaries. Moreover, rare inclusions which EDS revealed to be alumina were sometimes found within grains in the neighbourhood of dislocation configurations, such as shown on Fig. 2. No cavities were observed at triple points or grain boundaries in the as-received materials.

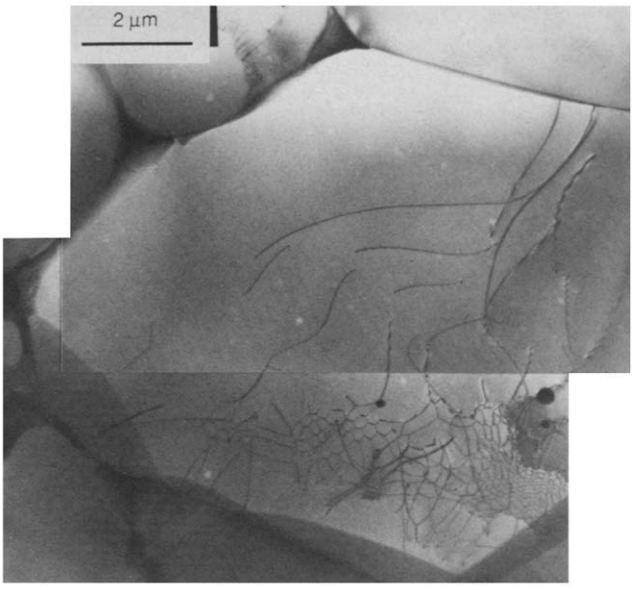

Fig. 2. As-received HPAlN. TEM bright field micrograph. The second phase appears with dark contrast at triple points. A few dislocations and a twist subgrain boundary can be seen. The last features are very seldom seen in as-received material.

Test samples for compressive creep and deformation experiments were diamond machined from the initial discs as $3 \times 3 \times 8\,mm^3$ bars the lengths of which lie in the disc planes.

The creep and CSR tests were performed in a MTS 810 machine equipped with a Centorr furnace, the samples being placed between two silicon carbide plates. All tests were conducted in a mixture of argon and helium gases from 1500 to 1650°C. Creep experiments in compression have been carried out under stresses of 150, 200 and 250 MPa and CSR tests at a strain rate of $5 \times 10^{-6}\,s^{-1}$. The deformation was recorded using a linear voltage differential transformer (LVDT) and the temperature measured by both a W/W–Rh thermocouple and a pyrometer pointing at the specimen. After cooling the deformed samples under stress, 3-mm diameter disks were diamond cut at an angle of 0, 45° or 90° from the compression axis. Thin foils could then be prepared as described before.

3 Results of Compression Tests

3.1 Creep curves

Creep curves, $\varepsilon = f(t)$ can usually be decomposed into three stages: 1, decreasing strain rate; 2, steady state strain rate and 3, increasing strain rate. Most creep experiments are interpreted considering only the steady state strain rate, $\dot{\varepsilon}$. It obeys an equation of the type:

$$\dot{\varepsilon} = A(T)\frac{\sigma^n}{d^p}$$

where σ is the applied stress, d is the grain size, n is the stress exponent, p is the grain size exponent, and

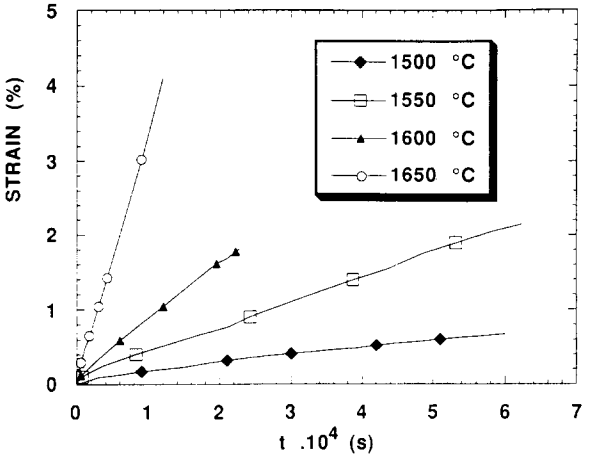

Fig. 3. Creep curves (strain versus time) of SPAlN compressed at 150 MPa from 1500°C to 1650°C.

$A(T)$ is often expressed as an Arrhenius factor, i.e. proportional to $\exp[-Q/RT]$, where R is the gas constant.

When the rate-controlling mechanism is diffusion, the steady-state creep rate, $\dot{\varepsilon}$, is proportional to the applied stress and inversely proportional to the square of the grain size, so $n = 1$ and $p = 2$.

Most of the present experiments were stopped during the second stage. For both materials studied, a stage 1 of very small duration followed by a well-characterized stage 2 were observed. The slope of the steady state, $\dot{\varepsilon}$, strongly increased with temperature: more than one order of magnitude from 1500 to 1650°C. Figure 3 shows the curves obtained for SPAlN deformed under 150 MPa. For the tests conducted under 250 MPa, after a time of 5000 s, which corresponds roughly to the beginning of the linear regime, strain varied from 0·2% at 1500°C to 4% at 1650°C for SAlN and 0·18% at 1500°C to 5% at 1650°C for HPAlN respectively.

Creep experiments were carried out for a minimum of 10 000 s which is the time required for contact with liquid steel in casting applications. At lower temperatures, tests were performed for times of about 60 000 s in order to have a better characterization of the second stage. One test was carried out on HPAlN at 1650°C which led to fracture after a deformation of 15%.

In order to determine the steady-state creep rate, strain rate versus strain was plotted for several temperatures under a constant stress. In most cases, between 0 and 0·2% strain, the rate quickly decreased and then reached a nearly constant value. In the cases of high stresses and temperatures, the rate decreased, went through a minimum and then slightly increased again. Figure 4 shows such behaviour for HPAlN under 250 MPa.

With the view of determining the influences of the applied stress and the temperature on steady-state creep rate, one value was chosen for each test. In

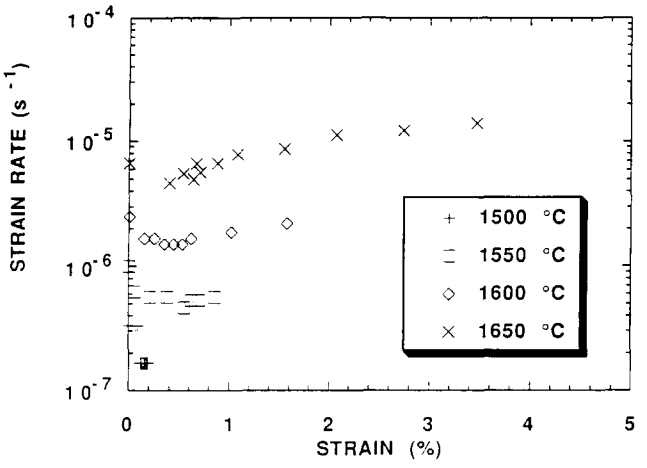

Fig. 4. Creep curves (creep rate versus strain) of HPAlN compressed at 250 MPa from 1500°C to 1650°C.

the general case, the minimum strain rate was taken as the steady-state creep rate. For high stresses and temperatures, the minimum of the curve was assumed to coincide with the steady-state creep. Thus, for both materials, the creep rate was typically between $6 \times 10^{-8}\,s^{-1}$ and $4 \times 10^{-6}\,s^{-1}$. The lowest creep rate that could be accurately measured with the present equipment was $10^{-8}\,s^{-1}$. At 1500°C and 150 MPa, the observed steady-state creep rate was nearly equal to this value. Log $\dot{\varepsilon}$ versus log σ curves were plotted for each material and temperature. The data could be fitted with straight lines. Table 1 gives the different values of the stress exponent, n, as a function of temperature.

The log $\dot{\varepsilon}$ versus $1/T$ data were plotted for a constant stress and for each material. From straight line fits of the data, the corresponding apparent activation energies could be estimated. Table 2 shows that these values do not depend on the stress in the investigated range except perhaps for HPAlN which yields a higher value at 150 MPa.

3.2 Constant strain rate curves

CSR tests were carried out on the one hand to determine the maximum stress and on the other hand to compare microstructural mechanisms with those found for creep. The strain rate was chosen in the domain of steady-state creep rate obtained before. The value of $5 \times 10^{-6}\,s^{-1}$ was selected for

Table 1. Stress exponents in AlN, derived from the stress dependence of the steady-state (or minimum) creep rate, at different temperatures

Temperature (°C)	*Stress exponent, n*	
	SAlN	*HPAlN*
1 500	1·8	1·8
1 550	1·8	1·4
1 600	1·4	1·4
1 650	1·2	1·4

Table 2. Apparent activation energies in AlN, derived from the temperature dependence of the steady-state (or minimum) creep rate, at different applied stresses

Stress (MPa)	*Activation energy (kJ/mol)*	
	SAlN	*HPAlN*
150	650	710
200	620	645
250	630	640

Table 3. Peak (or maximum) stresses observed in stress–strain curves of AlN deformed in compression at the imposed strain rate $\dot{\varepsilon}$ of $5 \times 10^{-6}\,s^{-1}$, at different temperatures

Temperature (°C)	*Stress (MPa)*	
	SAlN	*HPAlN*
1 500	580	—
1 525	515	—
1 550	480	670
1 600	330	430
1 650	185	290

reasons of accuracy. Stress–strain curves showed first a linear part with a high slope, then the stress reached a maximum and decreased.

The lower the temperature, the higher the slope of the initial part of the curve, the maximum stress and the slope of the decreasing part of the $\sigma(\varepsilon)$ recording. In Fig. 5, stress–strain curves are plotted for HPAlN at 1550, 1600 and 1650°C. For comparison, the curve of SAlN deformed at 1650°C was also added to Fig. 5. An initial slope and a maximum stress lower than those found for HPAlN in the same conditions were observed. Similar differences have also been observed at other temperatures. The values of maximum stresses are reported in Table 3.

Tests were stopped when strains were approximately the same as those obtained for creep except for one sample of SAlN deformed up to 11% at 1650°C without fracture.

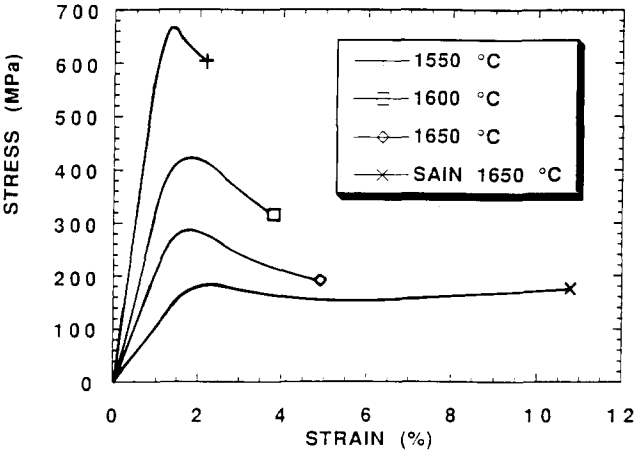

Fig. 5. Stress–strain curves of HPAlN compressed at a constant strain rate of $5 \times 10^{-6}\,s^{-1}$ from 1550°C to 1650°C and of SAlN compressed at $5 \times 10^{-6}\,s^{-1}$ and 1650°C.

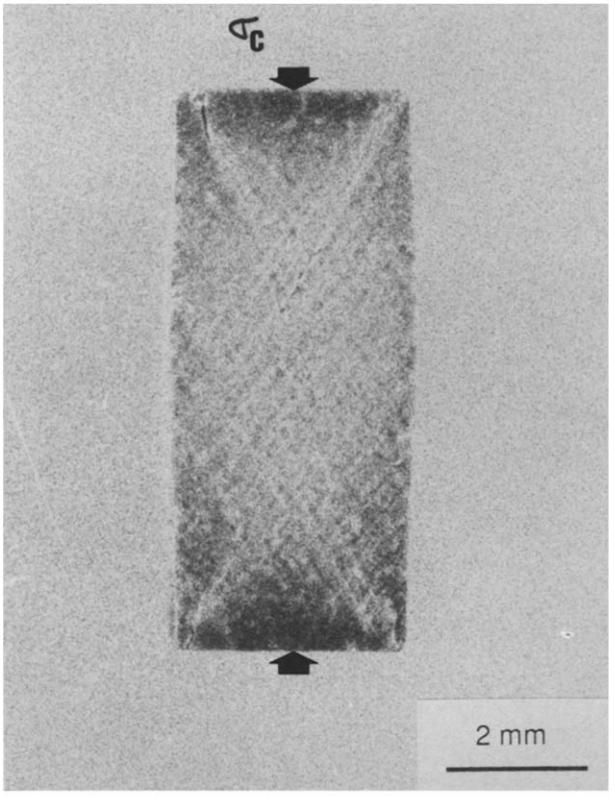

Fig. 6. Optical micrograph of a SAlN sample compressed at $\dot{\varepsilon} = 5 \times 10^{-6}\,s^{-1}$ at 1550°C up to 9·7% strain. The barrel shape is visible as well as deformation bands at an angle of 20° from the compression axis.

3.3 Microstructure

After creep, the samples still had a parallelepipedic shapes, while after CSR tests they had barrel shape and bands were observed at the sample surfaces at approximate angles of 20° to the compression axis (Fig. 6). In both materials and after both types of experiments, no clear evidence of significant modification in either grain size or grain shape was apparent upon SEM and TEM examinations. Grains are still equiaxed and their diameters measured on 200 grains are, for SAlN and HPAlN, respectively:

—For creep, $6{\cdot}5 \pm 2{\cdot}4\,\mu m$ and $5{\cdot}4 \pm 1{\cdot}8\,\mu m$.
—For CSR, $7{\cdot}6 \pm 2{\cdot}8\,\mu m$ and $5{\cdot}0 \pm 2{\cdot}0\,\mu m$.

A slight increase of grain size can, however, be noticed for HPAlN.

The first important result upon microscopic investigation was the observation of intergranular deformation and mostly cavitation. Cavities were observed at grain boundaries and triple points. Their locations were mostly observed in SEM on faces containing the compression axis. After creep, no evident correlation has been found between cavitation and the grain boundary orientations with respect to the compression axis (Fig. 7). In contrast, after CSR, an anisotropy was observed: the lower the angle between the grain boundary and the stress

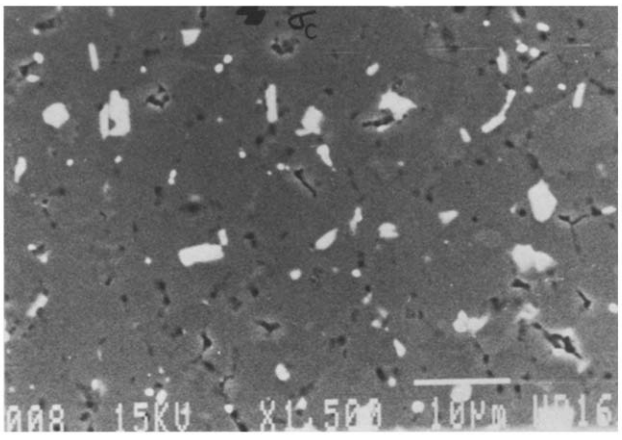

Fig. 7. SEM micrograph of HPAlN after creep at 200 MPa and 1550°C up to 0·9% strain. The second phase appears bright and cavities dark. The distribution of cavities looks isotropic without any relation to the compression axis.

axis the higher the probability for it to be affected by cavitation.

Figure 8 was taken on a lateral face of a SAlN sample deformed to 9·7% at 1550°C. Coalescence of cavities leading to microcracks more or less parallel to the stress axis could be noted as well as cavities localized at triple points. On SEM and mostly TEM observations, triple points cavities exhibited the shape of a convex triangle or a three-branched concave star (Fig. 9). Those cavities are reported as w-type according to the terminology of Garofalo.[6] TEM examinations also showed cavities located at grain boundaries which exhibit ellipsoidal shape with a main axis oriented along the grain boundary direction (Fig. 9). They are usually considered to be r-type cavities as described by Garofalo.[6]

When grain boundaries are very inclined to the thin foil plane, as observed in Fig. 10, cavities with a tube shape were observed crossing the foil from one face to the other. They are in fact ellipsoids. In general, in a grain boundary, cavities are regularly spaced, the

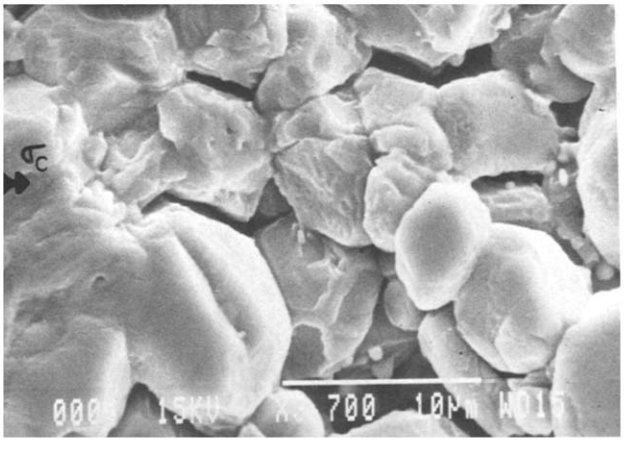

Fig. 8. SEM micrograph of SAlN after constant strain rate deformation at $5 \times 10^{-6}\,s^{-1}$ and 1550°C, final strain 9·7%. Side face of the sample is shown. Microcracks and cavities are preferentially oriented parallel to the horizontal compression axis.

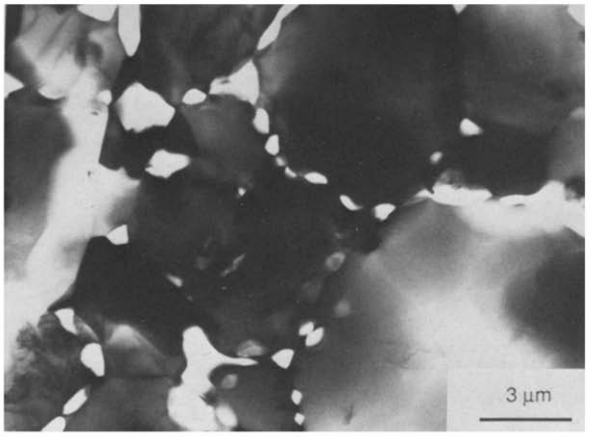

Fig. 9. TEM micrograph of HPAlN deformed at 250 MPa, 1650°C up to 4·2%. w- and r-type cavities are observed (see text), (bright field).

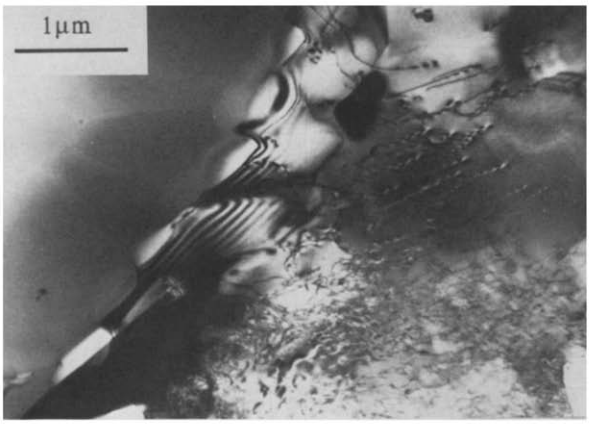

Fig. 10. TEM micrograph of HPAlN deformed at $\dot{\varepsilon} = 5 \times 10^{-6}\,s^{-1}$, 1550°C to 2·1% final strain. Cavities with tube shape and ellipsoidal basis run through the foil (bright field).

distance between them being of the order of magnitude of their main axis. Their sizes were determined by TEM; the diameter was taken as the largest dimension in the thin foil plane. For a given deformation condition, all cavities are about the same size. Their volume fraction was estimated during TEM observations. For a given area of about 700 μm^2, the total area taken up by cavities was calculated by adding individual areas. The ratio of these areas gives the volume fraction of cavities. The size and the volume fraction of cavities were mostly determined after deformation at the highest temperatures. The results are reported in Table 4.

In order to detect chemical changes of second phases, after creep and CSR, EDS analyses were made on second-phase particles located in the core of the samples. In all cases, the ratio Al/La was smaller after deformation. Before deformation, it was found to be equal to 10 but after creep, it could take the value of 2 after 78 min of testing at 1650°C under 250 MPa. After CSR, the decrease of the Al/La ratio was smaller; for example, after a deformation of 73 min, at 1600°C, it was equal to 7.

Several strain whorls have also been observed on non-cavitated grain boundaries, as described previously by Lange *et al.*[7] in deformed Si_3N_4. These concentric fringes are bend contours generated at one point of the grain boundary; they can appear in one or in the two adjacent grains (Fig. 11). They are

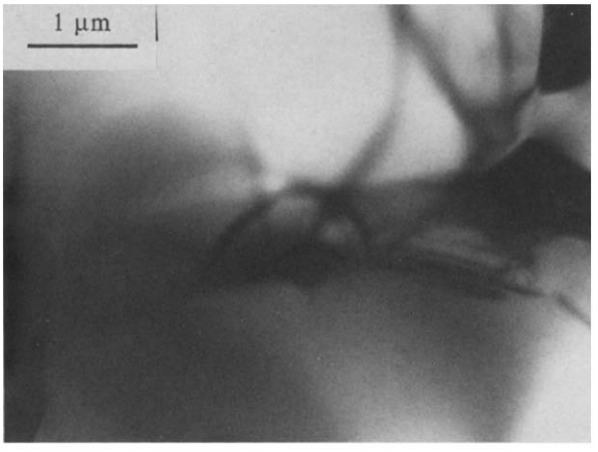

Fig. 11. TEM micrograph of SAlN after creep at 200 MPa, 1650°C, up to 3% strain. Strain whorl at a grain boundary (bright field).

manifestations of a localized elastic strain coming from residual stresses due to asperities which hindered grain boundary sliding.

Intragranular deformation was also observed. The proportion of grains with a high dislocation density increased with strain but not all the grains were concerned in any case. Dislocations have 1/3 $\langle 11\bar{2}0 \rangle$ Burgers vectors. No evidence of dissociation into partial dislocations was detected by the weak-beam technique. In most cases, the dislocation density is not homogeneous inside a

Table 4. Diameter and density of cavities observed by TEM in sintered and hot-pressed AlN for different testing conditions

Material	*Conditions of deformation*	*Average cavity diameter (μm)*	*Cavity density (%)*
SAlN	Creep (250 MPa, 1650°C) $\varepsilon = 3{\cdot}9\%$	1·0	3·0
	Creep (250 MPa, 1600°C) $\varepsilon = 2{\cdot}4\%$	1·0	4·0
HPAlN	Creep (250 MPa, 1650°C) $\varepsilon = 4{\cdot}2\%$	0·9	6·0
	Creep (250 MPa, 1600°C) $\varepsilon = 2{\cdot}3\%$	0·6	1·9
HPAlN	CSR ($5 \times 10^{-6}\,s^{-1}$, 1650°C) $\varepsilon = 4{\cdot}8\%$	0·7	5·7

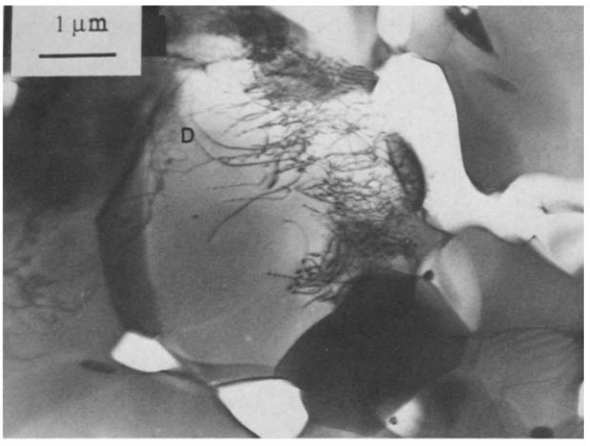

Fig. 12. TEM micrograph of HPAlN after creep at 250 MPa, 1650°C, up to 4·2% strain. Highly inhomogeneous dislocation distribution. The curvature of some dislocations (*D*) strongly suggests that they come from the grain boundary (bright field).

grain: it is maximum in the vicinity of the grain boundaries where the dislocation density can reach 10^{10} cm^{-2}; it decreases to almost zero as the distance from this point increases. As shown in Fig. 12, the dislocations are typically concentrated in one half of the grain. Since specimens were cooled under load, the curvature of dislocations gave indication on the direction of their displacement during high temperature deformation. When the dislocation density was very high, the shape of each dislocation could not be well defined; nevertheless, for each case of deformation, the sense of curvature has been identified. Figure 12 also showed dislocations (D) coming from the grain boundary which is the case most frequently observed and other ones going towards the grain boundary where the density is maximum. The interaction between dislocations gives rise to dense tangles and local hardening is probably high, which could prevent further deformation in such an area.

After creep or CSR for a maximum stress of 290 MPa, the configuration already described was always observed. In these cases, dislocation lines did not have a preferential crystallographic orientation.

Figures 13 and 14 were taken on grains where dislocations were rather homogeneously distributed and could be individually observed. As shown in Fig. 13 obtained from a thin foil with a more or less isotropic orientation some dislocations with a curved shape appear free to glide and contribute to the plastic strain whereas other ones (N) have interacted to form triple nodes which corresponds to the first steps of twist boundary formation. In Fig. 14, a typical configuration corresponding to the case where the basal plane is parallel to the electron beam can be seen. Two types of segments can be observed as:

—Straight lines parallel to the trace of the basal plane and which are projections of dislocation lines situated in the (0001) plane.
—Curved lines sometimes connecting two straight lines.

No preferred orientation was detected during observations on the basal plane. The dislocation lines being made of segments in the (0001) planes are connected by parts which are not located in defined prismatic planes.

This type of configuration results from basal glide, together with cross slipping on planes in zones with the Burgers vector ($(10\bar{1}0)$, $(10\bar{1}1)$) and also dislocation climb. In the particular sample that was stressed up to 670 MPa, the distribution of dislocations in grains was also heterogeneous but dislocation lines were oriented along particular directions.

Figure 15, for example, shows elongated loops lying on several non-basal planes. The longest segments are quite accurately parallel to the basal plane and have therefore a nearly pure screw character. The short segments also appear much

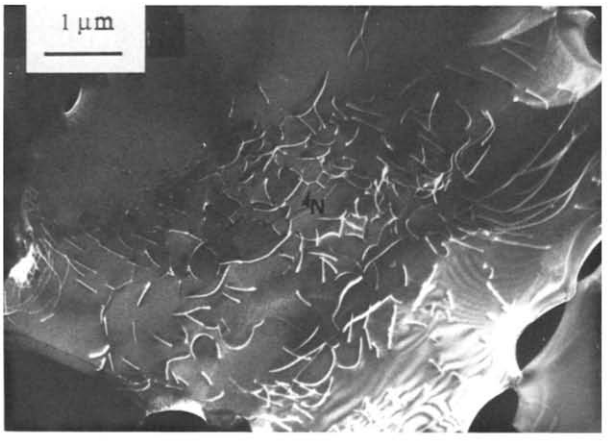

Fig. 13. TEM micrograph of HPAlN after creep at 250 MPa, 1600°C up to 2·3% strain. Dislocations are homogeneously distributed in the grain. Note the formation of triple nodes (N) by reactions dislocations. Weak beam conditions g, 2 g. g = $\bar{2}110$, foil normal and beam direction: [0001].

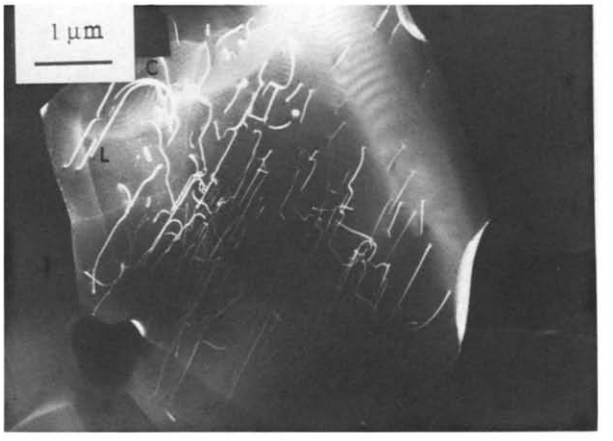

Fig. 14. TEM micrograph of SAlN after creep at 150 MPa, 1500°C, up to 0·7% strain. Long straight dislocation segments (L), parallel to the basal plane are linked by curved parts (C). Weak beam conditions g, 2 g. g: $\bar{2}110$, foil normal and beam direction: [$10\bar{1}0$].

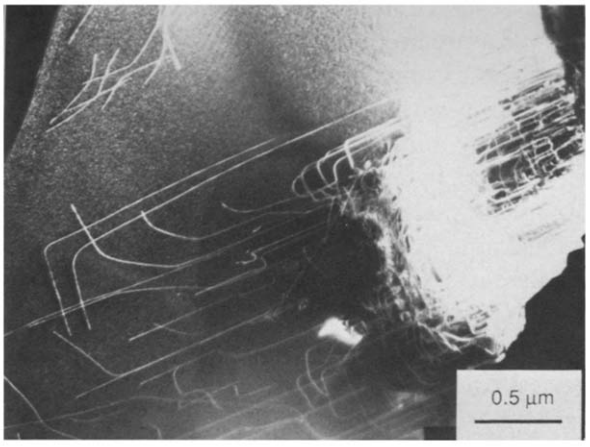

Fig. 15. TEM micrograph of HPAlN deformed 2·1% at $5 \times 10^{-6}\,s^{-1}$, 1650°C. Dislocation loops made of straight segments in non-basal planes. Long segments are parallel to the trace of the basal plane and have a nearly pure screw character. Weak beam conditions, 2g. g: $\bar{2}110$, foil normal and beam direction: $[10\bar{1}0]$.

more rectilinear than in samples deformed at lower stresses, although particular crystallographic orientations were not determined. Two of the three possible $\langle 11\bar{2}0\rangle$ Burgers vectors were usually observed inside a given grain. In Fig. 16, two such families of dislocations with dominant screw character can be seen. Most of long dislocations have cusps and some developed non-planar configurations with helicoidal character. Small loops in rows parallel to the screw orientations are also shown. They could be debris of screw dipoles that have been annihilated by cross-slip.

4 Discussion

The stress and temperature dependence of the 'steady-state' strain rate in creep, the origin of the maximum stress in constant strain rate experiments and the possible microscopic deformation mechanisms suggested by TEM and SEM observations are now discussed.

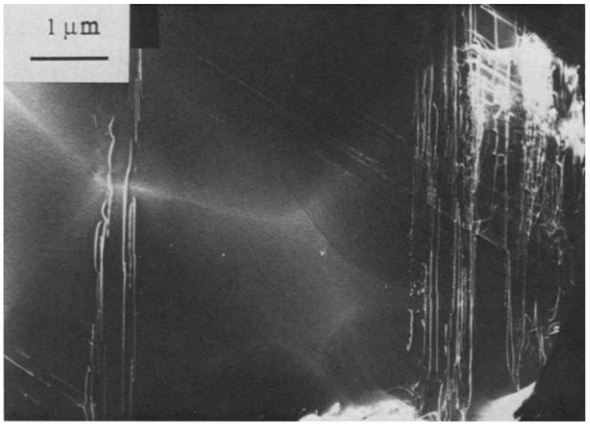

Fig. 16. TEM micrograph of HPAlN deformed 2·1% at $5 \times 10^{-6}\,s^{-1}$, 1650°C. Two sets of screw dislocations, parallel to two out of the three possible $\langle 11\bar{2}0\rangle$ directions are visible. Cusps on dislocations correspond to non-planar configuration resulting from cross-slip and/or climb. Rows of small loops parallel to the Burgers vector are also visible. Weak beam conditions g, 2 g. g: $2\bar{1}\bar{1}0$, foil normal and beam direction: [0001].

Creep curves were described with the classical phenomenologic parameters, n and Q. The stress exponent n, varying between 1·2 and 1·8 with an average value $\sim 1{\cdot}5$, is low compared to those commonly observed in most crystalline materials and predicted by current dislocation creep models, which range from ~ 3 to ~ 5. The apparent activation energy, Q, is rather large (625 kJ/mol = 6·48 eV) and the authors believe that is cannot be attributed to one single thermally activated mechanism. Such n, Q values are in agreement with literature results for ceramic materials tested in similar conditions. In AlN, the data obtained by Jou & Virkar[5] in four-point bending at somewhat lower stresses (20 to 140 MPa) and similar temperatures (1377 to 1667°C), favourably compare to the present values. These authors found two distinct Q values of ~ 530 and 625 kJ/mol for two different grain sizes 1·8 μm and 19 μm, respectively. Their stress exponent was measured at $\sim 1{\cdot}3$–$1{\cdot}4$. It is remarkable that the preparation process (sintering or hot pressing) does not influence the n, Q values much.

In constant strain rate tests, the maximum stress is highly sensitive to the deformation temperature. An apparent activation energy can be derived assuming the same form of the phenomenological constitutive equation, as for creep, which can be rewritten as:

$$\sigma \propto B\dot{\varepsilon}^{1/n} \exp\left(\frac{Q}{nkT}\right)$$

where σ could be the yield stress. If such derivation is done with σ equal to the maximum stress and $n = 1{\cdot}5$, the apparent activation energies are ~ 320 kJ/mol for SAlN and 375 kJ/mol for HPAlN. These estimates are clearly smaller than creep apparent activation energies. A probable reason is that the maximum stress on stress–strain curves does not have the same origin as the steady state creep and does not correspond to the comparable microstructural states.

The stress decrease after the maximum is probably due to some weakening, resulting from microcracks that formed parallel to the compression axis, rather than to an intrinsic softening. This maximum should not be confused with the yield drop due to dislocation multiplication which is commonly observed in single crystalline semiconductors, although crystallographic structures are very similar. A preferential orientation of cracks and cavities has been observed in polycrystalline magnesia.[8] A calculation by the same group[9] has shown that the traction stress perpendicular to the compression axis could amount to a tenth of the applied

stress because of end effects and barrel shape. This should lead to a more important density of cracks when the applied stress is larger, in agreement with the present observation of a steeper stress decrease at lower temperatures.

Microstructural observations strongly suggest that the dominant and initial deformation mechanism is intergranular and should be mainly grain boundary sliding (GBS), enhanced by the second phase, which is expected to be viscous at testing temperatures. Such a mechanism should account for a stress exponent of the order of 1. Due to defects along grain boundaries, even very small amounts of GBS lead to localized stress concentrations, which were termed 'whorls'[7] because of the fringe patterns they form on TEM micrographs. Such local defects with their surrounding stress fields are the nuclei for cavitation. The fact that many more cavities than 'whorls' were observed, contrarily to observations reported in Si_3N_4 ceramics[7,12] is due to a very fast cavity growth in the present material and testing conditions. Cavitation should relax internal stresses and suppress some obstacles to GBS but the way it contributes to the total strain is not obvious, especially in compressed samples where cavity distribution looks isotropic.

Intragranular deformation by dislocation movement is also a way to accommodate strain incompatibilities that result from GBS. Only limited deformation was observed in those grains which contained high dislocation densities. Dislocations were often confined in some grain boundary area and probably did not contribute significantly to the total strain.

The observed slip systems are those which were expected from the crystal structure. Only dislocations with $a = \langle 11\bar{2}0 \rangle$ basal Burgers vectors were observed. Dislocation configurations prove that $\langle a \rangle$ dislocations glide not only in (0001), but also in several non-basal planes, which unfortunately could not yet be identified. Cross-slip appears to be very easy, which is consistent with the non- or very narrow dissociation into Shockley partials. The present observations confirm those of Audurier *et al.*,[2,3] who deformed AlN samples containing yttrium oxides at higher stresses and lower temperatures.

The segmented appearance of dislocation loops developed at large stresses proves that high lattice friction (Peierls force) opposes dislocation motion, as in similar covalent crystals. It would be valuable to study in more detail the possible preferred non-screw orientations that seem to have been detected in the non-basal plane. The dominant screw character of dislocations was already observed in AlN at lower temperatures[2,3] and is a very general behaviour of dislocations in III.V semiconducting compounds.[11] In such materials, this is explained by a strong anisotropy of the dislocation mobility. One kind of edge-type dislocation moves much faster and trails behind it long slower screw segments. It should be interesting to check whether this is the reason for present observations or whether the screw orientation is not rather stabilized by accumulating jogs due to repeated cross-slip and/or climb. It should also be important to study more deformed AlN samples, in order to check whether the observed trend for increased dislocation activity with increasing strain can lead to a general plastic deformation by dislocations.

Acknowledgements

The assistance of A. Pianelli for XRD analysis of the second phases is gratefully acknowledged. This work was supported by IRSID (Research Institute of The French Iron & Steel Industry).

References

1. Heard, H. C. & Cline, C. F., Mechanical behaviour of polycrystalline BeO, Al_2O_3 and AlN at high pressure. *J. Mater. Sci.*, **15** (1980) 1889–97.
2. Audurier, V., Demenet, J. L. & Rabier, J., TEM study of dislocations in plastically deformed AlN. *Mater. Res. Soc. Symp. Proc.*, **242** (1992) 475–80.
3. Audurier, V., Demenet, J. L. & Rabier, J., Dislocation substructures in plastically deformed AlN. *Mater. Sci. Eng. A*, **164** (1993) 360–3.
4. Boch, P., Glandus, J. C., Jarrige, J., Lecompte, J. P. & Mexmain, J., Sintering oxidations and mechanical properties of hot pressed aluminium nitride. *Ceram. Int.*, **8** (1982) 34–40.
5. Jou, Z. C. & Virkar, A. V., High temperature creep and cavitation of polycrystalline aluminium nitride. *J. Am. Ceram. Soc.*, **73** (1990) 1928–35.
6. Garofalo, F., Déformation et rupture par fluage. Dunod, Paris, 1970, pp. 215–19.
7. Lange, F. F., Davis, B. I. & Clarke, D. R., Compressive creep of Si_3N_4/MgO alloys. *J. Mater. Sci.*, **15** (1980) 601–15.
8. Birch, J. M., King, P. J., Wilshire, B., Density changes during creep of polycrystalline MgO. *J. Mater. Sci.*, **10** (1975) 175–8.
9. Birch, J. M., Wilshire, B., Owen, D. J. R. & Shantaram, D., The influence of stress distribution on the deformation and fracture behaviour of ceramic materials under compression creep conditions. *J. Mater. Sci.*, **11** (1976) 1817–25.
10. Bernard-Granger, G., Duclos, R., Crampon, J. & Cales, B., High temperature creep properties of a Si_3N_4 ceramic related to the nature of the grain boundary phases. In *Proceedings Properties and applications of metallic and ceramic materials*, ed. M. H. Loretto & C. J. Beevers. MCF Publications, UK, 1992, 527–32.
11. Martinez-Hernandez, M., Kirchner, H. O. K., Korner, A., George, A. & Michel, J. P., Dislocations at grain boundaries in deformed silicon. *Phil. Mag. A*, **56** (1987) 641–58.